Experimental Neurology 322 (2019) 113044

Contents lists available at ScienceDirect

Experimental Neurology

journal homepage: www.elsevier.com/locate/yexnr

Research paper

Astrocyte-derived fatty acid-binding protein 7 protects blood-brain barrier integrity through a caveolin-1/MMP signaling pathway following traumatic brain injury

Qin Rui[a,1], Haibo Ni[b,1], Xiaolong Lin[c], Xiaojue Zhu[a], Di Li[d], Huixiang Liu[b,*], Gang Chen[e]

[a] Department of Laboratory, The Affiliated Zhangjiagang Hospital of Soochow University, Suzhou 215006, China
[b] Department of Neurosurgery, The Affiliated Zhangjiagang Hospital of Soochow University, Suzhou 215006, China
[c] Department of Orthopaedics, The Affiliated Zhangjiagang Hospital of Soochow University, Suzhou 215006, China
[d] Department of Translational Medicine Center, The Affiliated Zhangjiagang Hospital of Soochow University, Suzhou 215006, China
[e] Department of Neurosurgery & Brain and Nerve Research Laboratory, The First Affiliated Hospital of Soochow University, Suzhou 215006, China

ARTICLE INFO

Keywords:
FABP7
Caveolin-1
Astrocyte
Blood-brain barrier
Traumatic brain injury

ABSTRACT

The astrocyte-endothelial cell interaction is crucial for normal brain homeostasis and blood-brain barrier (BBB) disruption in pathological conditions. However, the mechanism by which astrocytes control BBB integrity, especially after traumatic brain injury (TBI), remains unclear. Here, we present evidence that astrocyte-derived fatty acid-binding protein 7 (FABP7), a differentiation- and migration-associated molecule, may function as a modulator of BBB permeability in a rat weight-drop model of TBI. Immunohistochemical analysis revealed that TBI induced increased expression of FABP7 in astrocytes, accompanied by caveolin-1 (Cav-1) upregulation in endothelial cells. Administration of recombinant FABP7 significantly ameliorated TBI-induced neurological deficits, brain edema, and BBB permeability, concomitant with upregulation of endothelial Cav-1 and tight junction protein expression, while FABP7 knockdown resulted in the opposite effects. Furthermore, pretreatment with daidzein, a specific inhibitor of Cav-1, reversed the inhibitory effects of recombinant FABP7 on matrix metalloproteinase (MMP)-2/9 expression and abolished its BBB protection after TBI. Altogether, these findings suggest that astrocyte-derived FABP7 upregulation may represent an endogenous protective response to BBB disruption partly mediated through a Cav-1/MMP signaling pathway following TBI.

1. Introduction

Traumatic brain injury (TBI) is defined as a head injury sustained from external force that destroys normal brain function (Nasser et al., 2016). Among a series of pathological changes after TBI, breakdown of the blood-brain barrier (BBB) is thought to be a crucial determinant of TBI severity and recovery time (Alluri et al., 2015; Jha et al., 2019; Robinson et al., 2018). Following trauma, BBB junctional proteins loosen and allow serum proteins such as albumin to leak into the brain parenchyma, which then trigger reactive astrocytes (Alvarez et al., 2013). Although reactive astrocytes often play a detrimental role in BBB disruption under pathological conditions, they may also exert protective effects on barrier function via expressing neurotrophic factors and cytokines, which are able to induce the restoration of endothelial junctional proteins (Cheslow and Alvarez, 2016; Ikeshima-Kataoka and Yasui, 2016). Thus, the identification of astrocytic factors that repair or protect BBB integrity might provide new insights into TBI therapy.

Fatty acid-binding protein 7 (FABP7), expressed by astrocytes in developing and mature brains, is a small cytoplasmic protein that serves as a cellular chaperone for lipophilic molecules (Matsumata et al., 2016; Zhang et al., 2018). By controlling the uptake and intracellular distribution of fatty acids, FABP7 is thought to be involved in metabolism, signal transduction and gene regulating activities (Kipp et al., 2011; Owada et al., 1996b). In the injured brain, FABP7 shows increased expression in astrocytes and is known as a trophic factor involved in astrocytic differentiation and migration, providing essential support for vascular morphology and function (Sharifi et al., 2011). However, the participation of FABP7 in BBB regulation, particularly during brain trauma, remains unidentified. Caveolin-1 (Cav-1) is the main structural protein of caveolae in the cell plasma membrane and is

* Corresponding author at: Department of Neurosurgery, The Affiliated Zhangjiagang Hospital of Soochow University, No.68 Jiyang Western Road, Suzhou 215006, China.
E-mail address: huixiangliu_zjg@163.com (H. Liu).
[1] Qin Rui and Haibo Ni contributed equally to this work.

https://doi.org/10.1016/j.expneurol.2019.113044
Received 21 April 2019; Received in revised form 15 August 2019; Accepted 23 August 2019
Available online 24 August 2019
0014-4886/

mostly found in brain endothelial cells and in low levels in astrocytes (Virgintino et al., 2002; Wang and Head, 2019; Zhao et al., 2014).In several models of adult brain injuries, Cav-1 is increased in the endothelium and has been shown to protect against BBB junctional protein degradation by reducing the proteolytic activity of matrix metalloproteinases (MMPs) in endothelial cells (Badaut et al., 2015; Gu et al., 2012; Nag et al., 2009). Interestingly, a recent study revealed that FABP7 was able to regulate the expression of Cav-1 to control lipid raft function in astrocytes (Kagawa et al., 2015). However, whether FABP7 plays a role in endothelial Cav-1 expression and its link to TBI-induced BBB disruption have yet to be explored.

Therefore, in this study, we tended to examine the expression profile of FABP7 and Cav-1 in the TBI brain using a weight-drop impact rat model and to further characterize the possible role and underlying mechanisms of FABP7 in the regulation of BBB permeability following TBI.

2. Materials and methods

2.1. Animals

Adult male Sprague-Dawley rats (n = 220, 250–280 g) were purchased from the Animal Center of Chinese Academy of Sciences (Shanghai, China). All work for this study was performed in accordance with the Animal Care and Use Committee of Soochow University. All rats were housed in a light and temperature-controlled room, with sufficient food and water.

2.2. Traumatic brain injury model

The TBI model was induced using Feeney's weight-drop model as previously described (Rui et al., 2018). First, adult male rats were intraperitoneally anesthetized with 4% chloral hydrate (400 mg/kg) and mounted in a stereotaxic frame. After the fur was shaved and routine disinfection was performed, a 5-mm-diameter craniotomy was performed at 3.5 mm posterior and 4 mm lateral to the bregma without laceration of the dura. Injury was delivered by releasing a steel rod (40 g weight) from a height of 25 cm onto a copper placed on the cranial dura, creating an impact depth of 2.5 mm. Then, the incision was closed with an interrupted 4–0 silk suture. Sham animals underwent the identical surgical procedures except the impaction. Body temperature was maintained at 37 °C using a heating pad throughout all procedures. After the surgical procedure was accomplished, animals were placed in a recovery chamber and then were transferred to their home cages.

2.3. Tissue collection and sectioning

Rats received an overdose of sodium pentobarbital (80 mg/kg; intraperitoneal (IP) injection) at the prescribed survival time and were transcardially perfused with 200 mL of 4 °C 0.9% saline or 200 mL phosphate-buffered saline (PBS) followed by 250 mL of ice-cold 4% paraformaldehyde. Then, tissue samples surrounding the contusion area that was located < 3 mm from the margin of the contusion site (or the region located < 3 mm from the parietal craniotomy in the sham-operated group) were collected on ice and rapidly frozen in liquid nitrogen until further use in messenger RNA (mRNA) and protein expression analyses (Fig. S1). For brain tissue sectioning, brains were steeped in 4% paraformaldehyde at 4 °C overnight and then cryoprotected with 15% and 30% sucrose. Then, 15-μm-thick brain sections between −2.12 mm bregma and − 4.80 mm bregma were collected using a microtome. Every fifth section beginning from a random start point was used for further staining by an investigator blinded to experimental conditions.

2.4. Study design and experimental groups

Four separate experiments were conducted in the present study (Fig. S2).

Experiment I

For the time-course analysis of endogenous FABP7 and Cav-1 after TBI, rats were randomly seperated into six groups as follows (n = 6/group): sham, 6, 12, 24, 48, and 72 h post TBI. Molecularly, real-time PCR and western blotting were used to detect the temporal expression levels of FABP7 and Cav-1. In addition, double immunofluorescence staining was applied to detect the cellular localization of target molecules at 24 h following TBI.

Experiment II

To assess the role of FABP7, recombinant FABP7 (rh-FABP7, Proteintech, United States) was prepared in dimethyl sulfoxide (DMSO) and injected intraperitoneally at doses of 5, 15 and 45 μg/kg 1 h after TBI induction. Rats were randomly divided into five groups: sham, TBI + vehicle, TBI + rh-FABP7 (5 μg/kg, L), TBI + rh-FABP7 (15 μg/kg, M), TBI + rh-FABP7 (45 μg/kg, H). Neurobehavioral scores were evaluated at 24 h, 3d, 7d, 14d after TBI in above groups (n = 12/group). In addition, brain edema and Evans blue (EB) extravasation were detected 24 h after TBI in the sham, TBI + vehicle, and TBI + rh-FABP7 groups (45 μg/kg, H) (n = 6/group).

Experiment III

In order to further explore the BBB protective effect of FABP7, small interfering RNA (siRNA) of FABP7 was administered by intracerebroventricular (ICV) injection at 24 h before TBI modeling. Rats were randomly divided into 5 groups: sham, TBI + vehicle, TBI + rh-FABP7 (45 μg/kg), TBI + scramble siRNA (TBI + si-Ctr), TBI + FABP7 siRNA (TBI + si-FABP7). Neurobehavioral tests were assessed at 24 h, 3d, 7d, 14d after TBI (n = 12/group). Brain edema, EB extravasation, western blot and double immunofluorescence were measured at 24 h after TBI (n = 6/group).

Experiment IV

To investigate the underlying relationship of FABP7 and Cav-1 on BBB function, Daidzein (0.4 mg /kg; Sigma-Aldrich, United States), a specific inhibitor of Cav-1 (Zhao et al., 2017), was administered by IP injection at 1 h before TBI modeling and then followed with rh-FABP7 (45 μg/kg) treatment. Rats were randomly divided into 5 groups (n = 6/group): sham, TBI + vehicle, TBI + rh-FABP7 (45 μg/kg), TBI + rh-FABP7 + DMSO, TBI + rh-FABP7 + daidzein. Western blot, immunofluorescence staining, and EB fluorescence were examined at 24 h after TBI.

2.5. Intracerebroventricular drug administration

For FABP7 in vivo knockdown, rat FABP7 siRNA (Guangzhou Ribo Biotechnology Co., Ltd., China) or scramble siRNA were administered at 24 h before TBI induction by ICV injection performed as previously described (Ni et al., 2018). The stereotactic ICV injection site was relative to bregma: 1.5 mm posterior; 1.0 mm lateral; 3.2 mm depth. Then, 500 pmol/5 μL siRNA were inserted into the ipsilateral ventricle using a 10-μL Hamilton syringe (Hamilton Company, United States) at a rate of 0.5 μL/min. After an additional 8 min, the needle was removed over a 3-min period, and the burr hole was sealed with bone wax. Target sequence: CCAAACCAACGGTGATTAT.

2.6. Real-time PCR

The total RNA of pericontusional cortex tissues was isolated using TRIzol Reagent (Invitrogen, United States) and spectrophotometric analysis (OD260/280 > 1.8) was used to ensure the purity and quantity of RNA. One microgram RNA for each sample was reverse-transcripted using SuperScript™ III Reverse Transcriptase Kit (Thermo Fisher, United States). Real-time-PCR analysis was conducted on QuantStudio™ Dx Real-Time PCR Instrument (Life Technologies Corporation, United States) using a PowerUp™ SYBR™ Green Master Mix kit (Thermo Fisher, United States) and corresponding primers. The expression levels for each gene were normalized to the endogenous control glyceraldehyde 3-phosphate dehydrogenase (GAPDH) mRNA level and presented as the fold change relative to the sham group ($2^{-\Delta\Delta CT}$). All samples were analyzed in triplicate. The primer sequences were synthesized by Invitrogen Life Technologies (Shanghai, China) and are exhibited as follows:

FABP7: F: 5′-GCAAGTGGGAAATGTGACCA-3′;
R: 5′-GTGTCCGGATCACCACTTTG-3′;
Cav-1: F: 5′-GCATCAGCCGTGTCTATTCC-3′;
R: 5′-TGCTGATGCGGATATTGCTG-3′;
GAPDH: F: 5′-TGGCCTTCCGTGTTCCTACC-3′;
R: 5′-CGCCTGCTTCACCACCTTCT-3′.

2.7. Western blot analysis

The pericontusional cortex tissues were homogenized and lysed in ice-cold RIPA buffer (Beyotime, China) with phosphatase inhibitor cocktails (Beyotime, China). The tissue homogenate was centrifuged at 12000 rpm for 20 min at 4 °C and the supernatant was stored at − 20 °C. The total protein concentrations were determined using a bicinchoninic acid (BCA) Protein Assay Kit (Thermo Fisher Scientific, Carlsbad, CA, USA). Proteins were separated using SDS-PAGE gel electrophoresis and transferred to polyvinylidene difluoride (PVDF) membranes (Millipore, United States), followed by blocking with 5% fat-free dry milk for 1 h at room temperature. The blots were then incubated with the following primary antibodies for 24 h at 4 °C: rabbit anti-FABP7 (1:1000, CST, United States), rabbit anti-Cav-1 (1:1000, Abcam, United States), mouse anti-claudin-5 (1:1000, Invitrogen, United States), rabbit anti-occludin (1:125, Invitrogen, United States), rabbit anti-zonula occludens-1 (ZO-1, 1:1000, Abcam, United States), rabbit anti-MMP-2 (1:1000, Abcam, United States), rabbit anti-MMP-9 (1:1000, Abcam, United States), chicken anti-albumin (1:1000, Abcam, United States), and rabbit anti-GAPDH (1:10,000, Sigma, United States). The next day, the PVDF membranes were washed with Tris-buffered saline-Tween (TBST) buffer for three times, and then were incubated with corresponding secondary antibodies, including goat anti-rabbit IgG-HRP (Invitrogen, United States), goat anti-mouse IgG-HRP (Invitrogen, United States) and goat anti-chicken IgG-HRP (Invitrogen, United States), for 2 h at 4 °C. The blots were finally probed with enhanced chemiluminescence (ECL) (Millipore, United States) and visualized with an imaging system (Bio-Rad, United States). The data of western blot were quantified by Image J software (National Institutes of Health, United States).

2.8. Immunofluorescence staining

Sections were washed three times in PBS with 0.3% Triton X-100 (PBST) for 5 min each and blocked with 10% goat serum (Gibco, USA) in PBST for 1 h at room temperature. The following primary antibodies were incubated at 4 °C overnight in 5% normal goat saline (NGS) in PBST: rabbit anti-FABP7 (1:500, CST, United States), rabbit anti-Cav-1 (1:500, Abcam, United States), mouse anti-claudin-5 (1:200, Invitrogen, United States), sheep anti- von Willebrand factor (vWF, 1:200, Abcam, United States), rabbit anti- vWF (1:400, Abcam, United States), rabbit anti-MMP-2 (1:200, Abcam, United States), rabbit anti-MMP-9 (1:500, Abcam, United States), and mouse anti- glial fibrillary acidic protein (GFAP, 1:200, Bio-Rad, United States). After washing the slides in PBS for three times, the corresponding fluorescence-conjugated secondary antibodies including Alexa Fluor 488 donkey anti-rabbit IgG antibody (1:1000, Invitrogen, United States) and Alexa Fluor 555 donkey anti-mouse IgG antibody (1:1000, Invitrogen, United States) were applied at room temperature for 1 h. As negative controls, sections were incubated without primary antibody. Slides were observed with a Leica DMi8 laser confocal microscope (Leica Microsystems, Germany) after counterstaining with 4′, 6-diamidino-2-phenylindole dihydrochloride (DAPI) for 10 min. The data were obtained from 30 randomly selected microscopic fields (six fields per section × five sections per rat) with LAS X software.

2.9. Neurological score

At 1, 3, 7, and 14 days after surgery, neurological function was assessed by two blinded examiners using the modified Garcia test and beam balance test. The modified Garcia test was used to comprehensive evaluate motor function, sensory function and autonomous movement. The scoring system included seven parameters including spontaneous activity, body proprioception, vibrissae touch, spontaneous movement of limbs, lateral turning, forelimb walking, and climbing wall of cage. Each subtest was scored from 0 to 3 (total 0–21 points) (Garcia et al., 1995). The beam balance test was used to assess deficits in the vestibular system. Rats were placed on a beam to walk for 1 min and detected deficits in the ability to balance. The score (0–4) was decided by the walking distance (Luong et al., 2011).

2.10. Brain water content

Brain edema was estimated using the wet/dry method. Briefly, at 24 h after TBI, the brains were quickly removed from the skull and separated into the ipsilateral cerebral hemisphere and the contralateral cerebral hemisphere. The sample was first weighed to determine the wet weight (WW) and then dried in an incubator at 105 °C for 72 h and reweighed to obtain the dry weight (DW). Brain water content was calculated using the following formula: brain water content = (WW-DW)/WW × 100%.

2.11. BBB permeability

BBB permeability was determined by measuring EB extravasation. At 2 h before the animals were euthanized, 2.5% EB dye (5 mL/kg; Sigma-Aldrich, United States) in saline was injected via the caudal vein. The right and left hemisphere brains were separately collected, rapidly weighed, homogenized in 50% trichloroacetic acid. After overnight incubation at 4 °C and centrifugation at 15,000 *g* for 30 min, 0.8 mL of the supernatant was measured for absorbance at 620 nm using a spectrophotometer. For EB fluorescence, after injected with EB dye, rats were intracardial perfused with 60 mL PBS and 60 mL 4% paraformaldehyde. Then the brains were removed and steeped in 4% paraformaldehyde at 4 °C for 24 h, followed by dehydrated with 15% and 30% sucrose. 15-μm-thick coronal sections were collected and were visualized using a laser confocal microscope Leica DMi8 (Leica Microsystems, Germany). The intensity of EB fluorescence was analyzed from 30 randomly selected microscopic fields (six fields per section × five sections per rat) with LAS X software.

2.12. Statistical analyses

All data were presented as the mean ± standard error of the mean (SEM). Analysis was performed using SPSS 18.0 software. For time course testing measurement, One-way analysis of variance (ANOVA) followed by Dunnett's post hoc test was used to determine individual group differences. For evaluation of behavioral data, two-way ANOVA

with repeated measurements followed by Dunnett's post hoc test was used to determine significant differences. For FABP7 and Cav-1-positive cell counts, a Student *t*-test was used to determine significant differences. Other data were analyzed using one-way ANOVA with Tukey's post hoc test to compare data from multiple groups. Statistical significance was defined as $P < .05$.

3. Results

3.1. Time course of endogenous FABP7 and Cav-1 expression after TBI

We first assessed the expression levels of endogenous FABP7 and Cav-1 during the acute phase of TBI. Real-time PCR and western blot analyses revealed that both mRNA and protein expression of FABP7 were significantly increased beginning at 12 h after TBI and reached a peak at 24 h after TBI. Following this peak, the level of FABP7 declined at 48 h, returning close to the normal level by 72 h after TBI (Fig. 1A, C; Fig. S5). Similar to the trend in FABP7 expression, the expression of Cav-1 mRNA and protein was also elevated after TBI, peaking at 24 h and then declining gradually but remaining higher than the expression in the sham group (Fig. 1B, D; Fig. S5).

3.2. Distribution of endogenous FABP7 and Cav-1 in the Peri-injury cortex after TBI

Then, we conducted double immunofluorescence staining to detect the distribution of FABP7 and Cav-1 with the neuronal marker NeuN, microglial marker CD11b, astrocytic marker GFAP, and endotheliocyte marker vWF. The results showed that the majority of FABP7-positive cells at 24 h after TBI were colabeled with GFAP (Fig. 2A) but not labeled with NeuN, CD11b, or vWF. In brain tissue, the number of FABP7-positive astrocytes was rare in sham animals and remarkably increased in the peri-injury cortex at 24 h after TBI (Fig. 2D). In addition, Cav-1-positive cells were mainly colabeled with vWF, and the immunoreactivity of Cav-1 in endotheliocytes was significantly increased at 24 h after TBI compared with that in the sham group (Fig. 2C, E).

3.3. Administration of exogenous FABP7 ameliorated neurological deficits, brain Edema, and BBB permeability after TBI

To verify whether upregulation of FABP7 was involved in TBI-induced brain injury, three different dosages of recombinant FABP7 protein (5, 15, or 45 μg/kg) were administered via IP injection at 1 h post trauma. The western blot results showed that rh-FABP7 treatment caused a significant increase in FABP7 expression in brain tissue from the perilesional area at 24 h post TBI (Fig. S6A). Neurological scores were evaluated at 1, 3, 7 and 14 days after TBI. As shown in Fig. 3A and B, rats in the vehicle groups showed significantly impaired neurological function in the Garcia test and beam balance test, whereas administration of rh-FABP7 at a dose of 45 μg/kg apparently improved the neurological evaluations at all tested time points. We then further determined the effects of recombinant FABP7 on brain edema and BBB

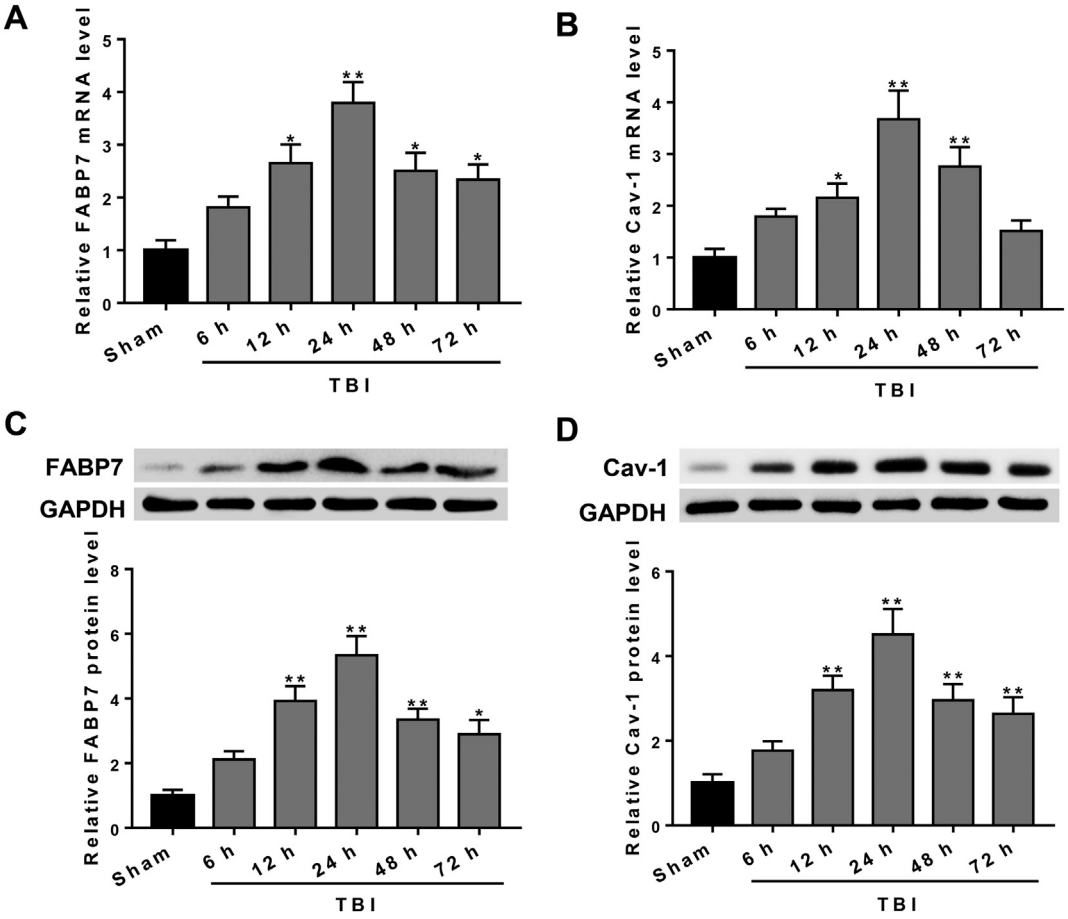

Fig. 1. Expression of endogenous FABP7 and Cav-1 in the peri-injury cortex after TBI. Quantitative real-time PCR analysis was performed to determine the relative expression levels of FABP7 (A) and Cav-1 (B) mRNA to GAPDH mRNA. The protein levels of endogenous FABP7 (C) and Cav-1 (D) in the sham and TBI groups were determined by western blot. The relative densities of each protein were normalized to those in the sham group. The expression levels of FABP7 and Cav-1 were increased at both the mRNA and protein levels after TBI. Statistical analyses were performed using one-way ANOVA followed by Dunnett's post hoc test. $n = 6$ for each group per time point. Data are expressed as the mean ± SEM. * $P < .05$, ** $P < .01$ vs. the sham group.

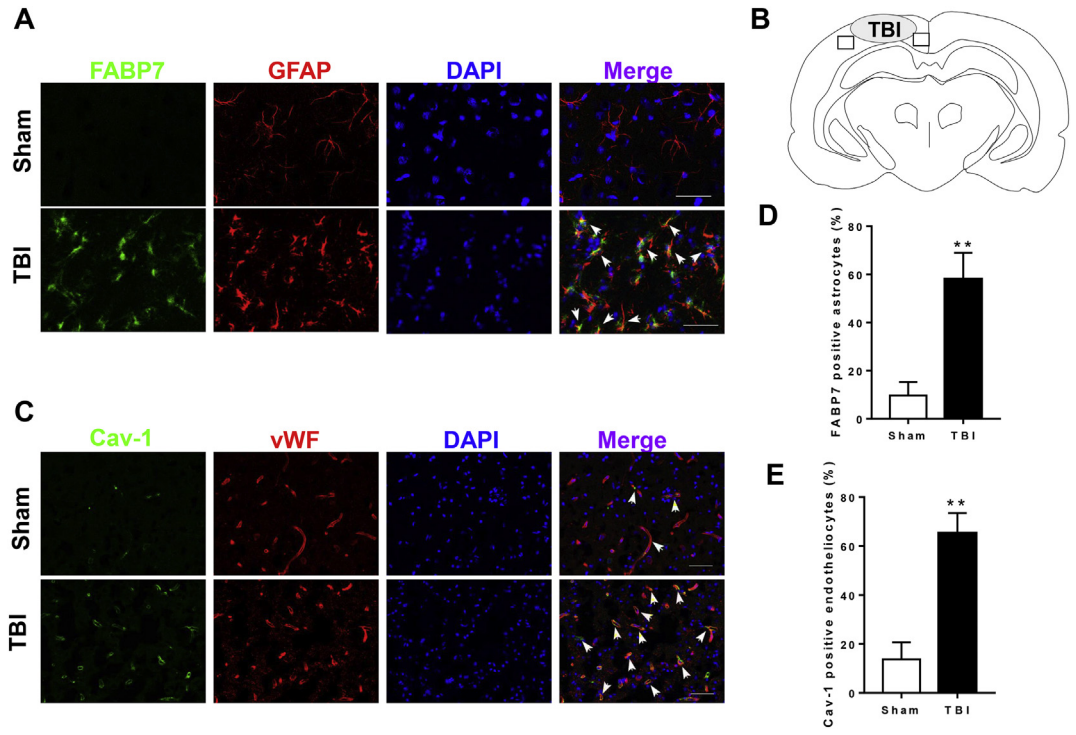

Fig. 2. Double immunofluorescence staining of FABP7 and Cav-1 in the peri-injury cortex after TBI. (A) Representative immunostaining images of FABP7 (green) with GFAP (red)-marked astrocytes to show expression profiles in the sham and 24-h TBI groups. (B) Schematic drawing of a coronal brain section. The squares indicate the detected areas of immunofluorescence staining analysis. (C) Representative immunostaining images of Cav-1 (green) with vWF (red)-marked endotheliocytes to show expression profiles in the sham and 24-h TBI groups. The nuclei were fluorescently labeled with DAPI (blue). The arrows indicate the colocalization of FABP7 and Cav-1. Scale bar = 50 μm. (D) Quantification of the number of FABP7-positive astrocytes. (E) Quantification of Cav-1-positive endotheliocytes. Statistical analyses were performed using Student's *t*-test; data are expressed as the mean ± SEM, n = 6 for each group; ** $P < .01$ vs. the sham group. (For interpretation of the references to colour in this figure legend, the reader is referred to the web version of this article.)

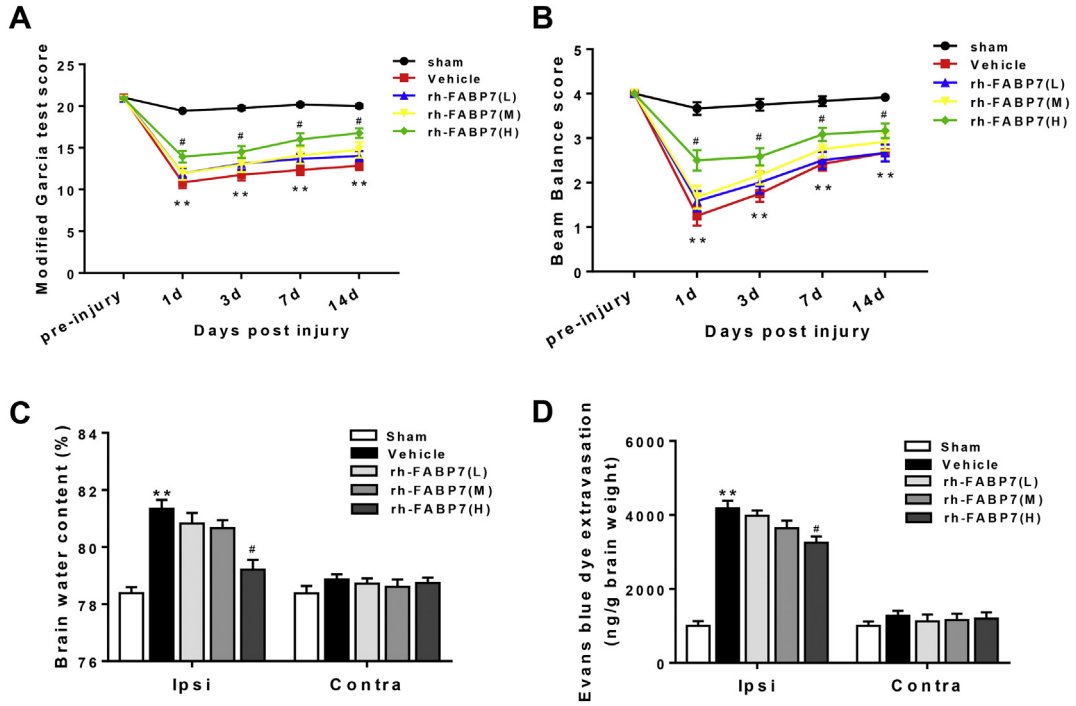

Fig. 3. Effects of exogenous FABP7 on neurological outcome, brain water content and BBB permeability after TBI. Neurological function was assessed using Garcia test score (A) and beam balance score (B) at 1, 3, 7, and 14 days after TBI; $n = 12$ for each group. Brain water content (C) and EB dye extravasation (D) were measured at 24 h after TBI; n = 6 for each group. Statistical analyses were performed using two-way ANOVA followed by Dunnett's post hoc test for neurobehavioral tests and one-way ANOVA followed by Tukey's post hoc test for other evaluation; data are expressed as the mean ± SEM,; ** $P < .01$ vs. the sham group; # $P < .05$ vs. the vehicle group. Ipsi indicates the ipsilateral injured hemispheres; Contra, contralateral uninjured hemispheres.

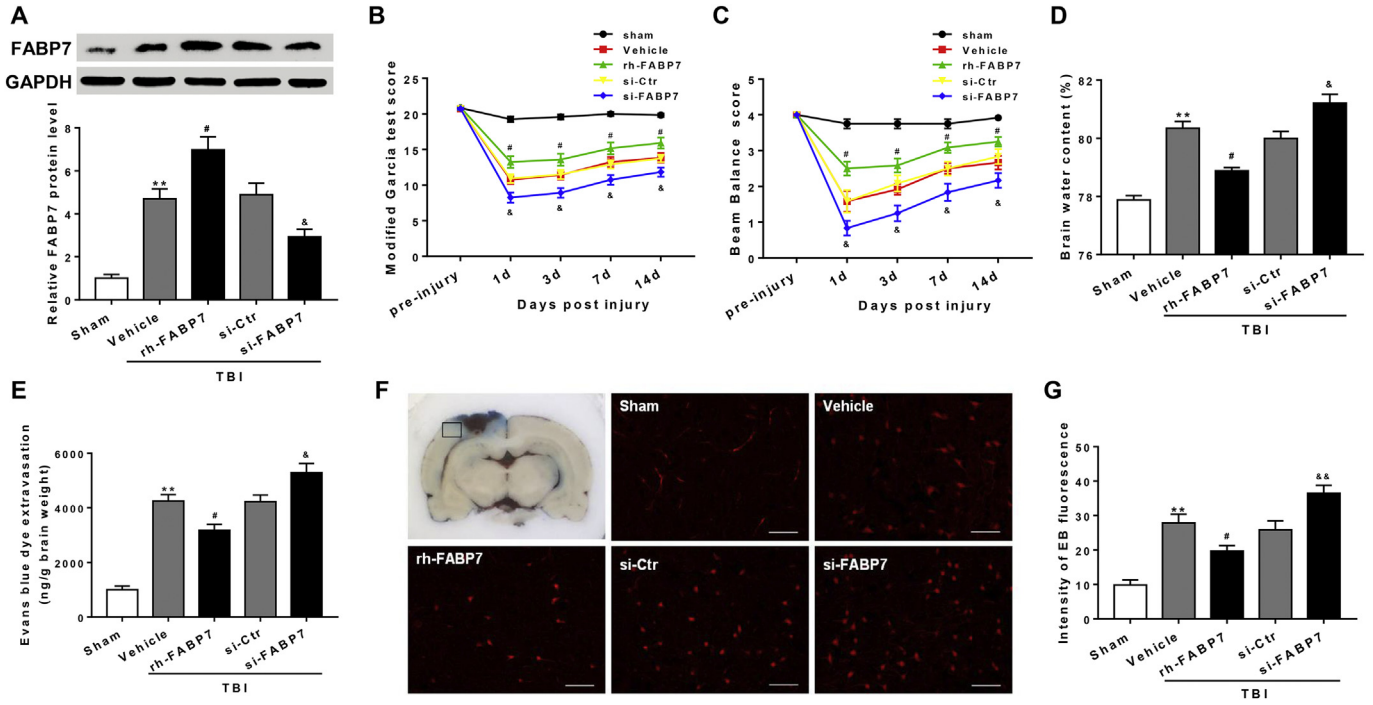

Fig. 4. Effects of FABP7 knockdown on BBB integrity after TBI. (A) Representative western blot images and quantitative analysis of FABP7 knockdown efficiency. The Garcia test score (B), beam balance score (C), brain water content (D), and EB extravasation (E) in the ipsilateral cerebral hemisphere are shown. (F) Representative fluorescent images of EB extravasation and quantitative analysis of the intensity of EB fluorescence in the peri-injury cortex. (G) Quantification of the relative fluorescence intensity of EB fluorescence is shown. Scale bar = 50 μm. Statistical analyses were performed using two-way ANOVA followed by Dunnett's post hoc test for behavioral tests and one-way ANOVA followed by Tukey's post hoc test for other evaluation; data are expressed as the mean ± SEM, n = 12 for the behavior tests in each group, n = 6 for the other tests in each group; ** $P < .01$ vs. the sham group; # $P < .05$ vs. the vehicle group; & $P < .05$, && $P < .01$ vs. the control siRNA (si-Ctr) group.

Permeability at 24 h after TBI. Brain water content and EB dye leakage in the ipsilateral hemisphere of the vehicle-treated TBI group was significantly increased compared with that in the sham group (Fig. 3C, D). However, this increase in brain edema and EB extravasation was significantly attenuated by 45 μg/kg rh-FABP7 treatment at 24 h post-TBI. Thus, we selected the highest dosage (45 μg/kg) of rh-FABP7 for the following studies.

3.4. Silencing of endogenous FABP7 aggravated neurological deficits, brain Edema and BBB permeability after TBI

To further evaluate the role of FABP7 in BBB integrity, specific FABP7 siRNA was administered by ICV injection 24 h before TBI induction. The western blot results showed that FABP7 expression at 24 h after TBI was efficiently knocked down by FABP7 siRNA pretreatment (Fig. 4A; Fig. S6B). Contrary to the effects of rh-FABP7, FABP7 siRNA significantly aggravated the neurological impairments from 1 to 14 days after TBI (Fig. 4B, C). Meanwhile, brain edema (Fig. 4D) and EB extravasation (Fig. 4E) in the ipsilateral cerebral hemisphere were significantly increased by FABP7 knockdown at 24 h after TBI. The EB fluorescence intensity in the peri-injury cortex (Fig. 4F, G) was consistent with the EB extravasation measured by spectrophotometry.

3.5. Effects of exogenous FABP7 and endogenous FABP7 deletion on vascular integrity after TBI

Vascular endothelial cells and tight junctions (TJs) are two major components of the BBB. We next evaluated the effects of FABP7 on the immunoreactivity of vWF (a marker of endothelial cells) and claudin-5 (a marker of TJs) using immunofluorescence staining. TBI causes a loss of vWF and claudin-5 immunoreactivity in brain tissue from the perilesional area. Treatment with rh-FABP7 rescued both the cellular localization of vWF and claudin-5. Conversely, FABP7 knockdown by siRNA further aggravated the loss of both immunoreactivities (Fig. 5A). To quantify these changes, low-magnification images of vWF and claudin-5 immunoreactivity in the peri-injury cortex were used for fluorescence intensity measurements. Consistent with the detection from high-magnification images, rh-FABP7 treatment significantly reduced vWF and claudin-5 degeneration, while its knockdown exerted the opposite effect (Fig. 5B-D). Additionally, in accordance with the immunostaining results, western blot analysis also showed loss of claudin-5 as well as other TJ proteins ZO-1 and occludin after TBI, and this loss was mitigated by rh-FABP7 treatment and further augmented by FABP7 knockdown (Fig. S3A-C).

3.6. Cav-1 inhibition abolished the protective effects of exogenous FABP7 on endothelial TJ proteins after TBI

Cav-1 has been reported to be involved in the stabilization of endothelial TJ proteins such as claudin-5, thereby protecting BBB integrity (Choi et al., 2016a; Choi et al., 2016b). We next focused on the effects of FABP7 on Cav-1 expression. As shown in Fig. S4A, rh-FABP7 treatment further increased TBI-induced Cav-1 overexpression. In contrast, FABP7 knockdown by siRNA significantly inhibited Cav-1 upregulation after TBI. To further confirm whether the protective effect of FABP7 on BBB integrity was mediated by Cav-1, daidzein, a specific inhibitor of Cav-1, was simultaneously administered by IP injection 1 h before TBI induction, followed by rh-FABP7 treatment in TBI rats. Western blot analysis showed that daidzein markedly decreased the Cav-1 protein level (Fig. 6A; Fig. S7); meanwhile, daidzein pretreatment also inhibited the increase in the expression of TJ proteins claudin-5, occludin and ZO-1 induced by rh-FABP7 (Fig. 6B; Fig. S4B, C). To provide direct evidence on the role of Cav-1 in FABP7-mediated TJ protein protection, we next conducted double immunofluorescence

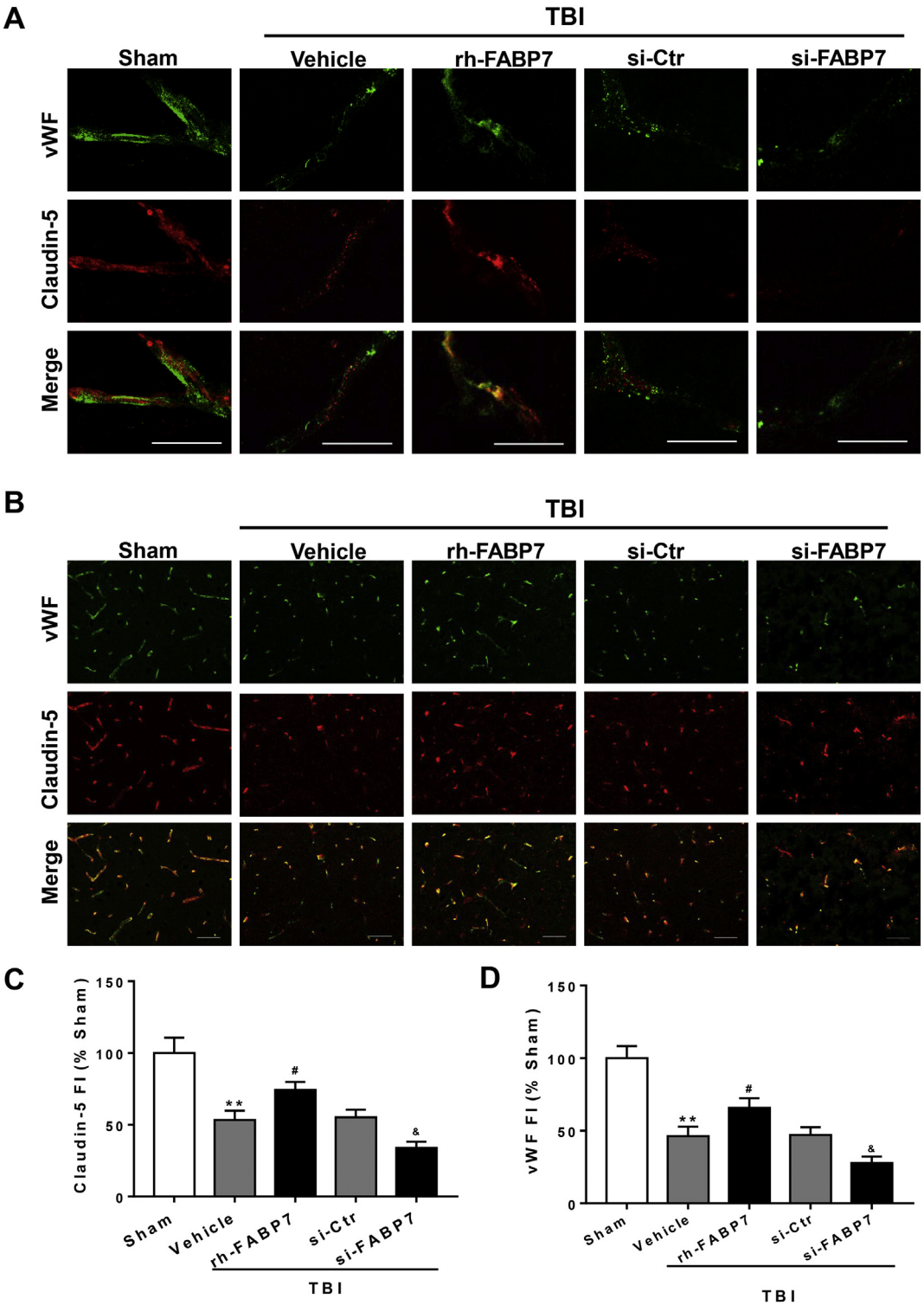

Fig. 5. Effects of exogenous FABP7 and endogenous FABP7 deletion on vascular integrity after TBI. (A) Representative high-magnification images of a cortical vessel immunostained for the endothelial cell marker vWF (red) and the TJ protein claudin-5 (red). Scale bar = 50 μm. (B) Low-magnification images demonstrating the extent of vWF and claudin-5 loss after TBI. Scale bar = 50 μm. Quantification of the relative fluorescence intensity of vWF (C) and claudin-5 (D) is shown below. Statistical analyses were performed using one-way ANOVA followed by Tukey's post hoc test; data are expressed as the mean ± SEM, n = 6 for each group; ** $P < .01$ vs. the sham group; # $P < .05$ vs. the vehicle group; & $P < .05$ vs. the si-Ctr group. (For interpretation of the references to colour in this figure legend, the reader is referred to the web version of this article.)

staining. As shown in Fig. 6C, postinjury treatment with rh-FABP7 presented increased Cav-1 immunoreactivity in the lesion site colabeled with rescued claudin-5 immunoreactivity. However, inhibiting endothelial Cav-1 immunoreactivity by daidzein pretreatment abolished the protective effect of rh-FABP7 on claudin-5 expression, as a significant reduction in its immunoreactivity was observed in the same location as Cav-1 (Fig. 6C-E).

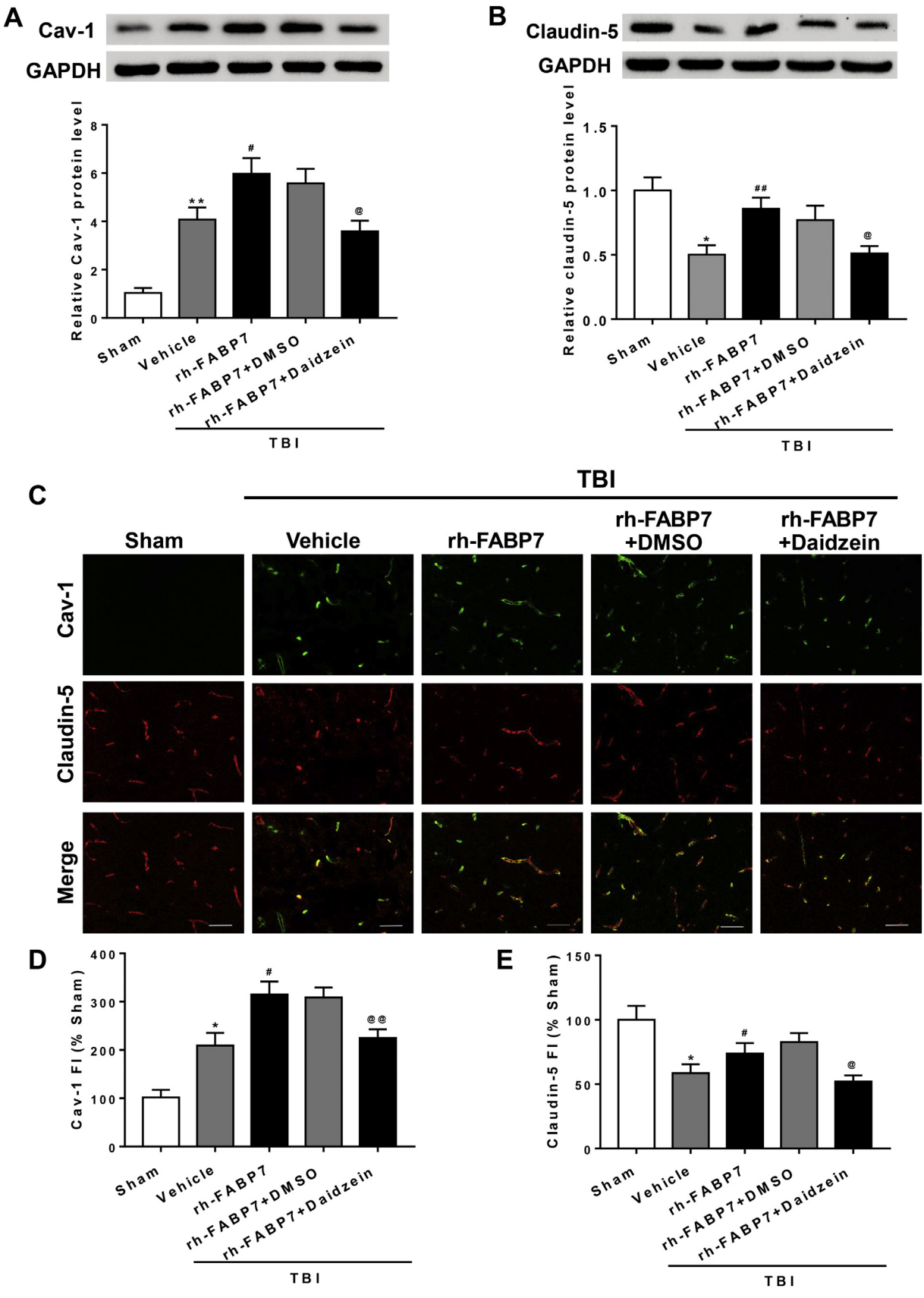

(caption on next page)

Fig. 6. Cav-1 inhibition abolished the protective effects of exogenous FABP7 on endothelial claudin-5 after TBI. TBI rats received an IP injection of daidzein (0.4 mg /kg) 1 h before trauma, followed by rh-FABP7 treatment as indicated. Western blot bands and quantitative analysis of Cav-1 (A) and claudin-5 (B) expression in the peri-injury cortex are shown. (C) Representative double immunofluorescence staining of Cav-1 (green) with claudin-5 (red) in the experimental groups. Scale bar = 50 μm. The relative fluorescence intensities of Cav-1 (D) and claudin-5 (E) are shown below. Statistical analyses were performed using one-way ANOVA followed by Tukey's post hoc test; data are expressed as the mean ± SEM, n = 6 for each group; * $P < .05$, ** $P < .01$ vs. the sham group; # $P < .05$, ## $P < .01$ vs. the vehicle group; @ $P < .05$, @@ $P < .01$ vs. the rh-FABP7 + DMSO group. (For interpretation of the references to colour in this figure legend, the reader is referred to the web version of this article.)

3.7. Cav-1 inhibition reversed the protective effects of exogenous FABP7 on MMP-2/9 expression and BBB permeability after TBI

Cav-1 is known to inhibit endothelial MMPs, which are key regulators of TJ protein degradation and BBB permeability during TBI (Gu et al., 2012; Jin et al., 2015). Therefore, we investigated whether the BBB-protecting effects of FABP7 may also involve MMPs in our model system. As evaluated by immunofluorescence staining and western blot, increased MMP-2 and MMP-9 expressions were observed in the peri-injury cortical vessel after TBI, and expressions of MMP-2 and MMP-9 were significantly reduced by rh-FABP7 treatment (Fig. 7A-D; Fig. S7). However, pretreatment with daidzein reversed the inhibitory effects of rh-FABP7 on MMP-2 and MMP-9 expression. In addition, consistent with the trend in MMP-2/9 expressions, daidzein pretreatment abolished the protective effects of rh-FABP7 on BBB permeability, as indicated by the increase in albumin level and EB leakage (Fig. 7E, F; Fig. S7).

4. Discussion

In the present study, we described a novel role of astrocyte FABP7 in protecting BBB integrity following TBI in rats. Our data showed that endogenous FABP7 expression was upregulated in astrocytes, which may have beneficial effects on BBB permeability, brain edema and neurological deficits after TBI. Such neurovascular protection by FABP7 was partly mediated by inducing endothelial Cav-1 overexpression, which in turn mitigated TJ protein degradation associated with MMP-2/9.

BBB disruption is one of the most frequently investigated mechanisms of TBI and has been commonly used to evaluate the degree and extent of brain injury (Daneman and Prat, 2015; Jha et al., 2019). Astrocytes are known to interact with endothelial cells via producing and secreting soluble factors such as retinoic acid (Mizee et al., 2014) and α-dystrobrevin (Lien et al., 2012) to induce vascular proliferation, angiogenesis, endothelial cell morphology, and ultimately influence the phenotype of the BBB under pathological conditions (Alvarez et al., 2013; Theis et al., 2005). FABP7, expressed by astrocytes in developing and mature brains, is known to bind with the highest affinity to docosahexaenoic acid (DHA), a polyunsaturated fatty acid of the n-3 family, and to be essential for neurogenesis as a positive regulator of proliferation in developing astrocytes in the brain (Kurtz et al., 1994; Owada et al., 1996a). Moreover, DHA has been demonstrated to prevent cerebrovascular EB leakage and brain edema following focal cerebral ischemia and spinal cord injury, suggesting a role for FABP7 in regulating BBB integrity (Hong et al., 2015; Samaddar, 2016). In the present study, we found that FABP7 was increased significantly in the early stage of TBI, and immunohistochemical observations showed that FABP7 was predominantly expressed in reactive astrocytes. These findings were consistent with previous reports showing elevated FABP7 levels in serum from patients with mild traumatic brain injury and acute ischemic stroke (Pelsers et al., 2004; Wunderlich et al., 2005). However, the expression profile of FABP7 and its cellular localization in the brain were not explored in these studies. Furthermore, several lines of evidence have confirmed that FABP7 is a key regulator of astrocytic function (Sharifi et al., 2011; Kamizato et al., 2019). In the stub-injured mouse brain, FABP7 showed increased expression in astrocytes and regulated the proliferative response of astrocytes by controlling fatty acid homeostasis (Sharifi et al., 2011). Most recently, FABP7 upregulation in astrocyte was reported to protect from the induction of inflammation leading to demyelination in a mouse model of multiple sclerosis (Kamizato et al., 2019). However, none of the previous studies have focused on the BBB regulation in relation to the neuroprotection induced by FABP7. Our study demonstrated that silencing endogenous FABP7 using siRNA exacerbated TJ proteins degradation accompanied by a leaky BBB and progressive development of brain edema. In contrast, recombinant FABP7 treatment significantly ameliorated these pathological processes following TBI. These results suggest that FABP7 may have a protective effect on BBB integrity following TBI.

Thus far, the exact molecular mechanism involved in FABP7-mediated BBB regulation remains unknown. Endothelial Cav-1, a major structural protein of caveolae, may be a good molecular candidate for studying changes in BBB permeability in response to astrocyte-derived factors because of its involvement in mediating the transcellular transport pathway (Deng et al., 2012). Cav-1 has also been shown to be involved in the stabilization of endothelial TJ proteins such as claudin-5, thereby protecting BBB integrity (Choi et al., 2016a; Choi et al., 2016b). In fact, increased expression of Cav-1 in the endothelium has been reported in several rodent models of brain injuries, including cold cortical injury, spinal cord injury, and brain ischemia (Jasmin et al., 2007; Nag et al., 2007; Shin, 2007). Silencing of Cav-1 can exacerbate the pathological damage in the BBB following injury (Jasmin et al., 2007). Consistent with the observations in a juvenile controlled cortical impact model (Badaut et al., 2015), the expression of Cav-1 at both the mRNA and protein levels was found to increase in vascular endothelial cells during the acute period following TBI in our present study. However, in a rat model of transient middle cerebral artery occlusion, Gu et al. obtained opposite results showing decreased Cav-1 expression at 24, 48 and 72 h in the in cortex microvessels of ischemic brain (Gu et al., 2012). In the same study, a decrease in Cav-1 expression was correlated with an increase in TJ protein degradation and enhanced BBB permeability in Cav-1 knockout mice (Gu et al., 2012). This discrepancy in Cav-1 expression might be due to differences in animal models, time points, focus areas, and experimental conditions. Interestingly, a recent study revealed that FABP7 regulated the expression of Cav-1 to control lipid raft function in astrocytes (Kagawa et al., 2015). FABP7 knockdown reduced the expression of Cav-1 at the protein and transcriptional levels in cultured astrocytes, and FABP7 re-expression in FABP7 knockout astrocytes rescued the decreased level of Cav-1 (Kagawa et al., 2015). In the present study, recombinant FABP7 treatment further augmented Cav-1 upregulation after TBI, while its knockdown exerted the opposite effect. Therefore, we plausible that the changes of Cav-1 expression in endothelial may be involved in BBB protection by FABP7 after TBI. To verify this hypothesis, we used daidzein, a specific inhibitor of Cav-1 protein (Zhao et al., 2017). As expected, daidzein significantly inhibited endothelial Cav-1 expression and reversed the protective effects of exogenous FABP7 on TBI-associated TJ protein degradation in endothelial cells. Together, these observations suggest that endothelial Cav-1 upregulation contributes to the FABP7-mediated BBB protection in TBI.

MMPs are proteolytic zinc-containing enzymes responsible for the rapid degradation of TJ proteins and the extracellular matrix around brain microvessels, subsequently leading to opening of the BBB(Galliera et al., 2015; Rempe et al., 2016; Yang et al., 2007). After TBI, excessive production of MMP-2/9 is a typical molecular event in the impairment

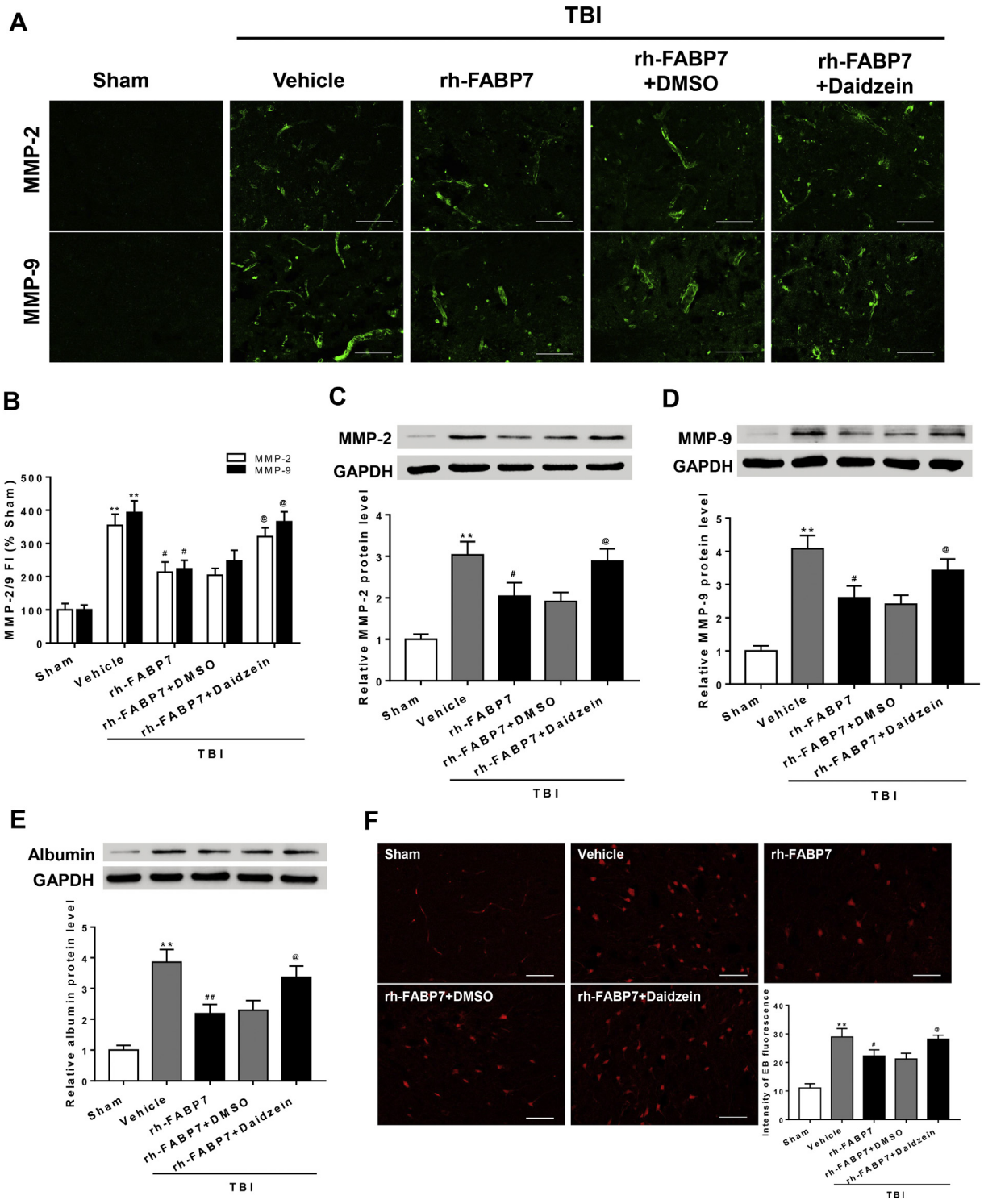

Fig. 7. Cav-1 inhibition reversed the protective effects of exogenous FABP7 on MMP-2/9 expression and BBB permeability after TBI. (A) Representative immunostained images for MMP-2 and MMP-9. Scale bar = 50 μm. (B) Quantification of the fluorescence intensity of MMP-2 and MMP-9 staining. Western blot bands and quantitative analysis of the MMP-2 (C), MMP-9 (D) and albumin levels (E) in the experimental groups are shown. (F) Representative fluorescent images of EB extravasation and quantitative analysis of the intensity of EB fluorescence in the peri-injury cortex. Scale bar = 50 μm. Statistical analyses were performed using one-way ANOVA followed by Tukey's post hoc test; data are expressed as the mean ± SEM, n = 6 for each group; ** $P < .01$ vs. the sham group; # $P < .05$, ## $P < .01$ vs. the vehicle group; @ $P < .05$ vs. the rh-FABP7 + DMSO group.

of TJ proteins and the associated dysfunction of the BBB (Abdul-Muneer et al., 2016). In fact, Cav-1 is considered as a key regulator of MMPs activity in cerebrovascular endothelial cells (Gu et al., 2012; Jin et al., 2015). During cerebral ischemia-reperfusion injury, the loss of endothelial Cav-1 initiates the activation of MMPs and secondary BBB disruption (Gu et al., 2012). In contrast, the re-expression of Cav-1 inhibited MMP-2/9 activation, promoted TJ protein recovery and decreased brain edema in Cav-1 knockout mice (Choi et al., 2016a). In agreement with these results, we also found that TBI induced a significant increase in MMP-2/9 expression, which was subdued by

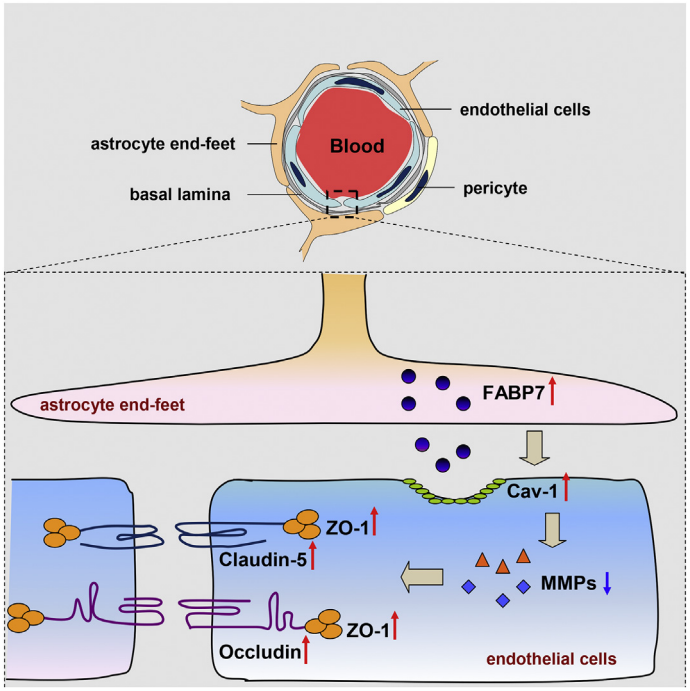

Fig. 8. Schematic representation of the possible mechanisms underlying FABP7-mediated neurovascular protection after TBI. Briefly, TBI induces a rapid increase in the production of FABP7, which may upregulate Cav-1 expression in endothelial cells. The increase of Cav-1 may inhibit the release of MMPs and the degradation of tight junction proteins by MMPs, which eventually alleviates BBB disruption.

exogenous FABP7. However, the pharmacological inhibition of Cav-1 reversed the protective effect of exogenous FABP7 on MMP-2/9 expression, accompanied by a worsening of BBB integrity after TBI. These findings suggest that the Cav-1/MMP signaling pathway is a part of the underlying protective mechanism of FABP7 on the BBB after TBI.

However, there are several limitations of this study that need to be mentioned. First, astrocyte-endothelial cell crosstalk is crucial to BBB function and is substantially modified following traumatic injury in the brain (Assis-Nascimento et al., 2018; Cheslow and Alvarez, 2016; Ikeshima-Kataoka and Yasui, 2016). Although our in vivo research identifies endothelial Cav-1 as a specific FABP7 target, we cannot rule out whether FABP7 contributes to BBB protection by other signaling pathways. In addition, Cav-1 has recently been reported to regulate oxidative stress in the vascular endothelium (Shiroto et al., 2014). Cav-1 knockdown by siRNA promotes a significant increase in endothelial reactive oxygen species production (Shiroto et al., 2014), which has been established to be detrimental and lead to major alterations in BBB structure and function following TBI (Pun et al., 2009). Thus, whether the antioxidant property of endothelial Cav-1 also plays a role in FABP7-mediated vasoprotection needs to be clarified in future studies.

In conclusion, the present findings indicate that astrocyte-derived FABP7 protects BBB integrity after TBI, which is associated with regulation of the Cav-1/MMP signaling pathway in endothelial cells (Fig. 8). Our study provides new insight into astroglial function in BBB control under pathological conditions and suggests that recombinant FABP7 may be an effective therapeutic strategy for TBI patients.

Supplementary data to this article can be found online at https://doi.org/10.1016/j.expneurol.2019.113044.

Ethics approval

All animal experiments are strictly in accordance with the guideline of Soochow University Institutional Animal Care and Use Committee.

Declaration of Competing Interest

No competing financial interests exist.

Acknowledgments

Declared none.

References

Abdul-Muneer, P.M., Pfister, B.J., Haorah, J., Chandra, N., 2016. Role of matrix metalloproteinases in the pathogenesis of traumatic brain injury. Mol. Neurobiol. 53, 6106–6123 (PMID: 26541883).

Alluri, H., Wiggins-Dohlvik, K., Davis, M.L., Huang, J.H., Tharakan, B., 2015. Blood-brain barrier dysfunction following traumatic brain injury. Metab. Brain Dis. 30, 1093–1104. 25624154.

Alvarez, J.I., Katayama, T., Prat, A., 2013. Glial influence on the blood brain barrier. Glia 61, 1939–1958 (PMID: 24123158).

Assis-Nascimento, P., Tsenkina, Y., Liebl, D.J., 2018. EphB3 signaling induces cortical endothelial cell death and disrupts the blood-brain barrier after traumatic brain injury. Cell Death Dis. 9, 7 (PMID: 29311672).

Badaut, J., Ajao, D.O., Sorensen, D.W., Fukuda, A.M., Pellerin, L., 2015. Caveolin expression changes in the neurovascular unit after juvenile traumatic brain injury: signs of blood-brain barrier healing? Neuroscience 285, 215–226 (PMID: 25450954).

Cheslow, L., Alvarez, J.I., 2016. Glial-endothelial crosstalk regulates blood-brain barrier function. Curr. Opin. Pharmacol. 26, 39–46 (PMID: 2648020).

Choi, K.H., Kim, H.S., Park, M.S., Kim, J.T., Kim, J.H., Cho, K.A., Lee, M.C., Lee, H.J., Cho, K.H., 2016a. Regulation of caveolin-1 expression determines early brain Edema after experimental focal cerebral ischemia. Stroke 47, 1336–1343 (PMID: 27012742).

Choi, K.H., Kim, H.S., Park, M.S., Lee, E.B., Lee, J.K., Kim, J.T., Kim, J.H., Lee, M.C., Lee, H.J., Cho, K.H., 2016b. Overexpression of caveolin-1 attenuates brain edema by inhibiting tight junction degradation. Oncotarget 7, 67857–67867 (PMID: 27708218).

Daneman, R., Prat, A., 2015. The blood-brain barrier. Cold Spring Harb. Perspect. Biol. 7, a020412 (PMID: 25561720).

Deng, J., Huang, Q., Wang, F., Liu, Y., Wang, Z., Wang, Z., Zhang, Q., Lei, B., Cheng, Y., 2012. The role of caveolin-1 in blood-brain barrier disruption induced by focused ultrasound combined with microbubbles. J. Mol. Neurosci. 46, 677–687 (PMID: 21861133).

Galliera, E., Tacchini, L., Corsi Romanelli, M.M., 2015. Matrix metalloproteinases as biomarkers of disease: updates and new insights. Clin. Chem. Lab. Med. 53, 349–355.

Garcia, J.H., Wagner, S., Liu, K.F., Hu, X.J., 1995. Neurological deficit and extent of neuronal necrosis attributable to middle cerebral artery occlusion in rats. Statistical validation. Stroke 26, 627–634.

Gu, Y., Zheng, G., Xu, M., Li, Y., Chen, X., Zhu, W., Tong, Y., Chung, S.K., Liu, K.J., Shen, J., 2012. Caveolin-1 regulates nitric oxide-mediated matrix metalloproteinases activity and blood-brain barrier permeability in focal cerebral ischemia and reperfusion injury. J. Neurochem. 120, 147–156 (PMID: 22007835).

Hong, S.H., Khoutorova, L., Bazan, N.G., Belayev, L., 2015. Docosahexaenoic acid improves behavior and attenuates blood-brain barrier injury induced by focal cerebral ischemia in rats. Exp. Transl. Stroke Med. 7, 3 (PMID: 25642315).

Ikeshima-Kataoka, H., Yasui, M., 2016. Correlation between astrocyte activity and recovery from blood-brain barrier breakdown caused by brain injury. Neuroreport 27, 894–900 (PMID: 27362437).

Jasmin, J.F., Malhotra, S., Singh Dhallu, M., Mercier, I., Rosenbaum, D.M., Lisanti, M.P., 2007. Caveolin-1 deficiency increases cerebral ischemic injury. Circ. Res. 100, 721–729 (PMID: 17293479).
Jha, R.M., Kochanek, P.M., Simard, J.M., 2019. Pathophysiology and treatment of cerebral edema in traumatic brain injury. Neuropharmacology 145, 230–246 (PMID: 30086289).
Jin, X., Sun, Y., Xu, J., Liu, W., 2015. Caveolin-1 mediates tissue plasminogen activator-induced MMP-9 up-regulation in cultured brain microvascular endothelial cells. J. Neurochem. 132, 724–730 (PMID: 25683686).
Kagawa, Y., Yasumoto, Y., Sharifi, K., Ebrahimi, M., Islam, A., Miyazaki, H., Yamamoto, Y., Sawada, T., Kishi, H., Kobayashi, S., Maekawa, M., Yoshikawa, T., Takaki, E., Nakai, A., Kogo, H., Fujimoto, T., Owada, Y., 2015. Fatty acid-binding protein 7 regulates function of caveolae in astrocytes through expression of caveolin-1. Glia 63, 780–794 (PMID: 25601031).
Kamizato, K., Sato, S., Shil, S.K., Umaru, B.A., Kagawa, Y., Yamamoto, Y., Ogata, M., Yasumoto, Y., Okuyama, Y., Ishii, N., Owada, Y., Miyazaki, H., 2019. The role of fatty acid binding protein 7 in spinal cord astrocytes in a mouse model of experimental autoimmune encephalomyelitis. Neuroscience 409, 120–129.
Kipp, M., Clarner, T., Gingele, S., Pott, F., Amor, S., van der Valk, P., Beyer, C., 2011. Brain lipid binding protein (FABP7) as modulator of astrocyte function. Physiol. Res. 1, S49–S60 (PMID: 21777034).
Kurtz, A., Zimmer, A., Schnutgen, F., Bruning, G., Spener, F., Muller, T., 1994. The expression pattern of a novel gene encoding brain-fatty acid binding protein correlates with neuronal and glial cell development. Development 120, 2637–2649 (PMID: 7956838).
Lien, C.F., Mohanta, S.K., Frontczak-Baniewicz, M., Swinny, J.D., Zablocka, B., Gorecki, D.C., 2012. Absence of glial alpha-dystrobrevin causes abnormalities of the blood-brain barrier and progressive brain edema. J. Biol. Chem. 287, 41374–41385 (PMID: 23043099).
Luong, T.N., Carlisle, H.J., Southwell, A., Patterson, P.H., 2011. Assessment of motor balance and coordination in mice using the balance beam. J. Vis. Exp. 49, 2376.
Matsumata, M., Inada, H., Osumi, N., 2016. Fatty acid binding proteins and the nervous system: their impact on mental conditions. Neurosci. Res. 102, 47–55 (PMID: 25205626).
Mizee, M.R., Nijland, P.G., van der Pol, S.M., Drexhage, J.A., van Het Hof, B., Mebius, R., van der Valk, P., van Horssen, J., Reijerkerk, A., de Vries, H.E., 2014. Astrocyte-derived retinoic acid: a novel regulator of blood-brain barrier function in multiple sclerosis. Acta Neuropathol. 128, 691–703 (PMID: 25149081).
Nag, S., Venugopalan, R., Stewart, D.J., 2007. Increased caveolin-1 expression precedes decreased expression of occludin and claudin-5 during blood-brain barrier breakdown. Acta Neuropathol. 114, 459–469 (PMID: 17687559).
Nag, S., Manias, J.L., Stewart, D.J., 2009. Expression of endothelial phosphorylated caveolin-1 is increased in brain injury. Neuropathol. Appl. Neurobiol. 35, 417–426 (PMID: 19508446).
Nasser, M., Bejjani, F., Raad, M., Abou-El-Hassan, H., Mantash, S., Nokkari, A., Ramadan, N., Kassem, N., Mondello, S., Hamade, E., Darwish, H., Zibara, K., Kobeissy, F., 2016. Traumatic brain injury and blood-brain barrier cross-talk. CNS Neurol. Disord. Drug Targets 15, 1030–1044 (PMID: 27528468).
Ni, H., Rui, Q., Xu, Y., Zhu, J., Gao, F., Dang, B., Li, D., Gao, R., Chen, G., 2018. RACK1 upregulation induces neuroprotection by activating the IRE1-XBP1 signaling pathway following traumatic brain injury in rats. Exp. Neurol. 304, 102–113 (PMID: 29518365).
Owada, Y., Yoshimoto, T., Kondo, H., 1996a. Increased expression of the mRNA for brain- and skin-type but not heart-type fatty acid binding proteins following kainic acid systemic administration in the hippocampal glia of adult rats. Brain Res. 42, 156–160 (PMID: 8915595).
Owada, Y., Yoshimoto, T., Kondo, H., 1996b. Spatio-temporally differential expression of genes for three members of fatty acid binding proteins in developing and mature rat brains. J. Chem. Neuroanat. 12, 113–122 (PMID: 9115666).
Pelsers, M.M., Hanhoff, T., Van der Voort, D., Arts, B., Peters, M., Ponds, R., Honig, A., Rudzinski, W., Spener, F., de Kruijk, J.R., Twijnstra, A., Hermens, W.T., Menheere, P.P., Glatz, J.F., 2004. Brain- and heart-type fatty acid-binding proteins in the brain: tissue distribution and clinical utility. Clin. Chem. 50, 1568–1575 (PMID: 15217991).
Pun, P.B., Lu, J., Moochhala, S., 2009. Involvement of ROS in BBB dysfunction. Free Radic. Res. 43, 348–364 (PMID: 19241241).
Rempe, R.G., Hartz, A.M., Bauer, B., 2016. Matrix metalloproteinases in the brain and blood-brain barrier: versatile breakers and makers. J. Cereb. Blood Flow Metab. 36, 1481–1507 (PMID: 27323783).
Robinson, B.D., Isbell, C.L., Shaji, C.A., Kurek Jr., S., Regner, J.L., Tharakan, B., 2018. Quetiapine protects the blood-brain barrier in traumatic brain injury. J. Trauma Acute Care Surg. 85, 968–976 (PMID: 29985239).
Rui, Q., Ni, H., Gao, F., Dang, B., Li, D., Gao, R., Chen, G., 2018. LRRK2 contributes to secondary brain injury through a p38/Drosha Signaling pathway after traumatic brain injury in rats. Front. Cell. Neurosci. 12, 51 (PMID: 29545743).
Samaddar, S., 2016. Effect of docosahexaenoic acid (DHA) on spinal cord injury. Adv. Neurobiol. 12, 27–39 (PMID: 27651246).
Sharifi, K., Morihiro, Y., Maekawa, M., Yasumoto, Y., Hoshi, H., Adachi, Y., Sawada, T., Tokuda, N., Kondo, H., Yoshikawa, T., Suzuki, M., Owada, Y., 2011. FABP7 expression in normal and stab-injured brain cortex and its role in astrocyte proliferation. Histochem. Cell Biol. 136, 501–513 (PMID: 21938553).
Shin, T., 2007. Increases in the phosphorylated form of caveolin-1 in the spinal cord of rats with clip compression injury. Brain Res. 1141, 228–234 (PMID: 17275798).
Shiroto, T., Romero, N., Sugiyama, T., Sartoretto, J.L., Kalwa, H., Yan, Z., Shimokawa, H., Michel, T., 2014. Caveolin-1 is a critical determinant of autophagy, metabolic switching, and oxidative stress in vascular endothelium. PLoS One 9, e87871 (PMID: 24498385).
Theis, M., Sohl, G., Eiberger, J., Willecke, K., 2005. Emerging complexities in identity and function of glial connexins. Trends Neurosci. 28, 188–195 (PMID: 15808353).
Virgintino, D., Robertson, D., Errede, M., Benagiano, V., Tauer, U., Roncali, L., Bertossi, M., 2002. Expression of caveolin-1 in human brain microvessels. Neuroscience 115, 145–152 (PMID: 12401329).
Wang, S., Head, B.P., 2019. Caveolin-1 in stroke neuropathology and neuroprotection: a novel molecular therapeutic target for ischemic-related injury. Curr. Vasc. Pharmacol. 17, 41–49 (PMID: 29412114).
Wunderlich, M.T., Hanhoff, T., Goertler, M., Spener, F., Glatz, J.F., Wallesch, C.W., Pelsers, M.M., 2005. Release of brain-type and heart-type fatty acid-binding proteins in serum after acute ischaemic stroke. J. Neurol. 252, 718–724 (PMID: 15834650).
Yang, Y., Estrada, E.Y., Thompson, J.F., Liu, W., Rosenberg, G.A., 2007. Matrix metalloproteinase-mediated disruption of tight junction proteins in cerebral vessels is reversed by synthetic matrix metalloproteinase inhibitor in focal ischemia in rat. J. Cereb. Blood Flow Metab. 27, 697–709 (PMID: 16850029).
Zhang, W., Chen, R., Yang, T., Xu, N., Chen, J., Gao, Y., Stetler, R.A., 2018. Fatty acid transporting proteins: roles in brain development, aging, and stroke. Prostaglandins Leukot. Essent. Fat. Acids 136, 35–45 (PMID: 28457600).
Zhao, Y.L., Song, J.N., Zhang, M., 2014. Role of caveolin-1 in the biology of the blood-brain barrier. Rev. Neurosci. 25, 247–254 (PMID: 24501156).
Zhao, Y., Pang, Q., Liu, M., Pan, J., Xiang, B., Huang, T., Tu, F., Liu, C., Chen, X., 2017. Treadmill exercise promotes neurogenesis in ischemic rat brains via Caveolin-1/VEGF Signaling pathways. Neurochem. Res. 42, 389–397 (PMID: 27747480).